Versatile Rigid-Fluid Coupling for Incompressible SPH

Nadir Akinci* University of Freiburg
Markus Ihmsen* University of Freiburg
Gizem Akinci* University of Freiburg
Barbara Solenthaler† ETH Zürich
Matthias Teschner* University of Freiburg

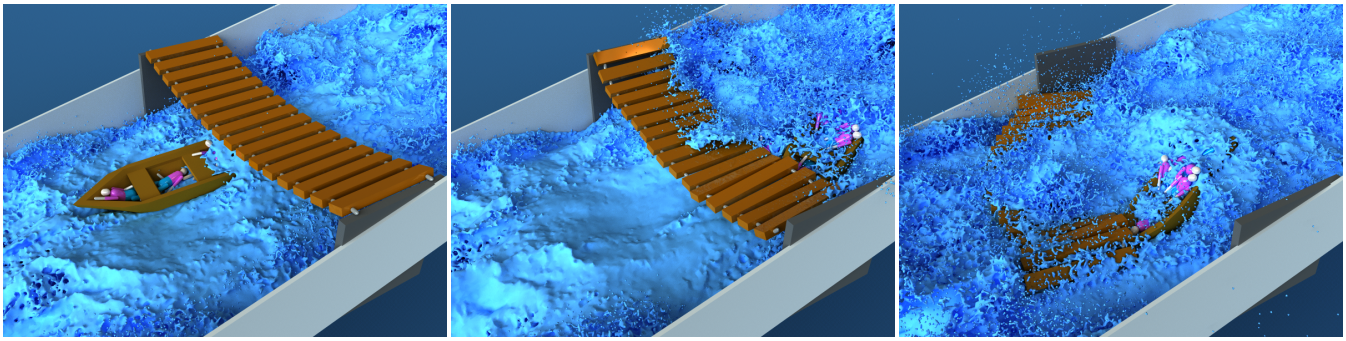

Figure 1: *Fluid-rigid interaction in a large-scale setting. A boat with ragdolls passes a bridge (left). A second boat with ragdolls collides with the bridge due to an increased flow rate and the bridge is released (middle and right).*

Abstract

We propose a momentum-conserving two-way coupling method of SPH fluids and arbitrary rigid objects based on hydrodynamic forces. Our approach samples the surface of rigid bodies with boundary particles that interact with the fluid, preventing deficiency issues and both spatial and temporal discontinuities. The problem of inhomogeneous boundary sampling is addressed by considering the relative contribution of a boundary particle to a physical quantity. This facilitates not only the initialization process but also allows the simulation of multiple dynamic objects. Thin structures consisting of only one layer or one line of boundary particles, and also non-manifold geometries can be handled without any additional treatment. We have integrated our approach into WCSPH and PCISPH, and demonstrate its stability and flexibility with several scenarios including multiphase flow.

CR Categories: I.3.7 [Computer Graphics]: Three-Dimensional Graphics and Realism—Animation;

Keywords: physically-based animation, fluid simulation, Smoothed Particle Hydrodynamics, fluid-solid coupling

Links: DL PDF VIDEO

*e-mail: {nakinci,ihmsen,gakinci,teschner}@informatik.uni-freiburg.de
†e-mail: solenthaler@inf.ethz.ch

1 Introduction

Lagrangian fluid simulation is a popular topic in computer animation. Its particle-based nature allows simulating small scale phenomena, while mass conservation is trivially satisfied. Recent works have addressed the performance issues of incompressible simulations, turning SPH into a competitive tool to model hydrodynamic effects. For instance, [Solenthaler and Pajarola 2009] has presented a prediction-correction method to eliminate compression artifacts efficiently. Other improvements in this context have been presented in [Bodin et al. 2011; Raveendran et al. 2011]. In addition, the efficiency of SPH can be further improved by including multi-scale concepts [Adams et al. 2007; Solenthaler and Gross 2011] and elaborated data structures for neighbor queries [Ihmsen et al. 2011].

The interesting fluid behavior, however, emerges when rigid objects are added to a simulation (see Figure 1). While the two-way coupling of particle-based fluids and solids seems to be straightforward, there is no general agreement how this should be handled. On one hand, the coupling has to cope with particle deficiency issues at the boundary in order to prevent spatial and temporal discontinuities of physical properties of the particles and sticking artifacts [Ihmsen et al. 2010] (see Figure 2). On the other hand, lower dimensional geometries, e.g. thin structures and non-manifold surfaces, as well as constrained rigid bodies should be supported. This work addresses these open issues. In the remainder of this section, we first discuss existing methods for treating boundaries in SPH (Section 1.1) as well as for rigid-fluid coupling (Section 1.2), and then highlight our contribution (Section 1.3).

1.1 Boundary Handling in SPH

For SPH boundary handling, distance-based penalty methods with boundary particles have been commonly used [Müller et al. 2004; Monaghan 2005; Harada et al. 2007; Monaghan and Kajtar 2009]. These approaches, however, require large penalty forces that restrict the time step. Furthermore, particles tend to stick to the boundary due to the lack of fluid neighbors. In [Harada et al. 2007], this problem is alleviated by employing a wall weight function for approximating density contributions for planar boundaries.

The sticking of particles is avoided with frozen and ghost particles

based models, e.g. [Libersky and Petschek 1991; Hu and Adams 2006]. Frozen particles are fluid particles which are constrained to static positions, whereas ghost particles are mirrored across the boundary on the fly. In order to guarantee non-penetration, either more than one layer of frozen particles should be used [Dalrymple and Knio 2001], or the positions of penetrating particles should be corrected [Ihmsen et al. 2010]. Since this class of methods samples the boundary with fluid particles, the relevant field variables can be well approximated with SPH. This results in continuous pressure gradients, which consequently prevents sticking of fluid particles to the boundaries. However, handling the interaction of the fluid with thin shells is problematic in these approaches since the elevated density on one side of a boundary particle affects potential fluid particles on the other side. The interaction of fluids with deformable thin shells has been demonstrated in [Lenaerts and Dutré 2008] with additional distance-based non-symmetric forces to prevent the penetration of fluid particles.

Alternative to particles, boundaries can also be efficiently represented with triangles. In this case, however, it is challenging to handle discontinuous surface normals and non-manifold structures that cause spatial and temporal discontinuities of the fluid properties.

1.2 Two-Way Fluid-Rigid Coupling in SPH

For the two-way coupling of SPH fluids and rigid bodies, only few approaches have been proposed so far. In [Clavet et al. 2005], the fluid is considered as a collection of rigid spheres exchanging impulses with surrounding rigid bodies. In [Oger et al. 2006; Keiser et al. 2006], the pressure at the boundary is taken into account for two-way coupled fluid-rigid interaction. In those models, however, dynamic forces, e.g. viscosity, are neglected. More recently, an impulse-based approach for simulating the two-way coupling of SPH fluids with particle-based rigid bodies has been proposed in [Oh et al. 2009]. This approach, however, is not purely based on hydrodynamic forces, relies on normal information for rigid bodies, and does not guarantee non-penetration for thin shells.

In [Becker et al. 2009b], direct forcing has been employed for both one- and two-way fluid-rigid coupling. This method uses a predictor-corrector scheme to compute forces that constrain particle positions and velocities to specific values. Non-penetration is guaranteed by using position correction. Different slip conditions are realized by including a non-symmetric friction model. The position correction and the non-symmetric friction forces are, however, not momentum-conserving. Another issue is that timestep-dependent operations are used that require careful parameter evaluation for each setup. Finally, it requires two additional neighbor queries for two-way coupling, which is rather expensive. This method has not yet been extended to handle the interaction of a particular fluid particle with multiple rigid bodies or the simultaneous contact among the bodies.

Particle-based fluid and deformable object interaction has been presented in [Müller et al. 2004] where the coupling has been realized with the Lennard-Jones potential, but without hydrodynamic forces. Boundary particles are automatically generated per triangle based on Gaussian quadrature. Deformations can also be computed with SPH as shown in e.g. [Solenthaler et al. 2007; Lenaerts and Dutré 2008; Becker et al. 2009a]. This has been extended to simulate porous flow in [Lenaerts et al. 2008]. Further, fluid-deformable interaction on GPUs has also been briefly discussed in [Allard et al. 2011].

There exist impressive two-way coupling approaches for Eulerian and semi-Lagrangian schemes (e.g. [Carlson et al. 2004; Guendelman et al. 2005; Chentanez et al. 2006; Batty et al. 2007; Robinson-Mosher et al. 2008]), as well as for 2D heightfield models (e.g. [Chentanez and Müller 2010]). A thorough discussion of these methods is, however, beyond the scope of our paper.

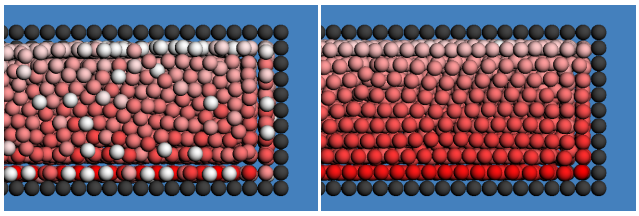

Figure 2: *Pressure profile of a box filled with particles where the front side is clipped for illustration purposes. The fluid particle pressures are color-coded and proportional to their red saturation. Black particles denote boundary particles. While [Becker et al. 2009b] leads to pressure noise and sticking artifacts (left), our method avoids these problems (right).*

1.3 Contributions

We present a novel, versatile method for the two-way coupling of SPH fluids and rigid bodies. We use boundary particles to sample the surface of rigid objects, which has several benefits. First, the use of particles allows us to derive a model that can cope with different shapes, including lower-dimensional rigid bodies consisting of one layer (referred to as thin shells) or one line of boundary particles (referred to as rods), as well as non-manifold geometries. Second, the inclusion of boundary particles successfully alleviates the particle deficiency problem of SPH near boundaries, preventing density (and consequently pressure) discontinuities at the boundary and particle sticking artifacts.

Our model addresses the problem of inhomogeneous particle sampling at the boundary by deriving new equations that consider the relative contribution of a boundary particle to a physical quantity. This does not only facilitate the particle initialization at complex boundaries, but also enables the use of multiple dynamic objects where the boundary sampling in the neighborhood may change due to contacts. A friction model is additionally included to simulate various slip conditions and drag effects. All pressure and viscous forces that are applied between fluid and boundary particles are symmetric, conserving linear and angular momentum. The approach is designed such that even very large density ratios between fluids and rigid bodies can be handled.

2 Fluid-Rigid Coupling

This section starts with a brief introduction of SPH in Section 2.1, followed by a description of our scheme for a corrected density computation at the rigid-fluid interface in Section 2.2. Sections 2.3 and 2.4 describe novel pressure and friction forces for pairs of boundary and fluid particles, while Section 2.5 discusses the overall forces and the symmetry of these forces.

2.1 SPH Concept

In SPH, a generic field variable A at position $\mathbf{x}_i$ is approximated using a finite set of sampling points $\mathbf{x}_j$ located within a distance $\|\mathbf{x}_i - \mathbf{x}_j\| < h$ as

$$A(\mathbf{x}_i) = \sum_j V_j A_j W(\mathbf{x}_i - \mathbf{x}_j, h), \tag{1}$$

where V_j is the volume represented at $\mathbf{x}_j$ and $W(\mathbf{x}_i - \mathbf{x}_j, h)$, also written as W_{ij}, denotes a Gaussian like kernel function with support radius h. The derivatives of A can be computed by using the derivatives of W in the interpolation.

In SPH simulations, density is one of the essential field variables that is used to compute pressure and viscosity forces. For this purpose, the density summation approach is commonly used, which reads as

$$\rho_i = \sum_j V_j \rho_j W_{ij} = \sum_j m_j W_{ij}. \tag{2}$$

In order to compute the pressure from the density, we either employ PCISPH [Solenthaler and Pajarola 2009] or WCSPH [Monaghan 2005; Becker and Teschner 2007]. The employed pressure and viscosity forces are based on [Monaghan 2005]. For generating surface tension effects, we rely on [Becker and Teschner 2007]. Finally, for simulating multiphase fluids, we use [Solenthaler and Pajarola 2008].

2.2 Corrected Density Computation

The density summation approach (2) approximates the density of a fluid particle correctly only if a particle is spherically surrounded by particles with the same initial density. Therefore, densities of fluid particles near the boundaries are underestimated. In order to alleviate this underestimation, we apply the Shepard filter [Panizzo 2004] to the density field. Even though this simple correction scheme significantly improves the situation, the density gradient still remains discontinuous near the boundaries. Additionally, since the particles near the boundaries do not have neighbors that spherically surround them, forces on such particles constrain their movements to the boundaries, which causes sticking artifacts. To avoid this problem, we take the neighboring boundary particles into account when computing densities and forces for fluid particles, similar to [Ihmsen et al. 2010].

Since we focus on the interaction of fluids with non-deformable rigid bodies without melting effects, particles do not necessarily need to be generated inside a rigid. Therefore, we generate particles as a single layer at the surface similar to [Bell et al. 2005; Becker et al. 2009a; Ihmsen et al. 2010]. This approach saves memory and improves performance. The particle representations of rigid bodies in the framework are computed either directly (e.g. for analytical shapes) or from mesh representations. Particle representations of triangle meshes are generated based on [Bell et al. 2005], which permits placing particles at an arbitrary offset to the surface mesh and yields a quite homogenous sampling. However, at high-curvature regions of the mesh, the particle distribution usually remains non-homogenous, resulting in a denser sampling in such areas (e.g., see Figure 3). We observed similar issues using the remeshing algorithm of [Botsch and Kobbelt 2004] and placing particles at the vertex positions. Fortunately, neither of the algorithms results in undersampled regions. Now, we can say that each boundary particle b_i represents a volume V_{b_i} at the surface of a rigid:

$$V_{b_i} = \frac{m_{b_i}}{\rho_{b_i}} = \frac{m_{b_i}}{\sum_k m_{b_k} W_{ik}},$$

where k denotes boundary particle neighbors. In [Solenthaler and Pajarola 2008], it has been shown that the density summation approach in (2) causes stability issues for large density ratios due to erroneous density estimations for particles at the interface. Therefore, the density of a fluid particle can be written as

$$\rho_{f_i} = m_{f_i} \sum_j W_{ij} + m_{f_i} \sum_k W_{ik}, \tag{3}$$

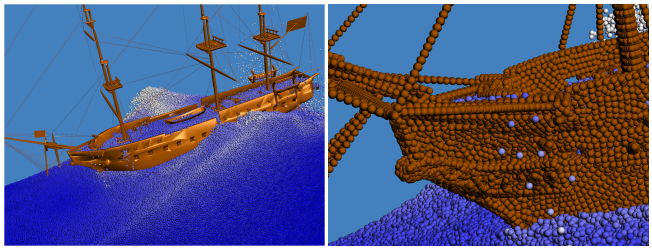

Figure 3: *A frigate is sailing on wavy sea. The right image shows the irregular sampling of boundary particles.*

where j denotes fluid particle neighbors. Applying this idea to the volume of a boundary particle results in

$$V_{b_i} = \frac{m_{b_i}}{m_{b_i} \sum_k W_{ik}} = \frac{1}{\delta_{b_i}}, \tag{4}$$

with $\delta_{b_i} = \sum_k W_{ik}$. Finally, (4) implies that the volume of a boundary particle gets smaller for densely sampled areas and larger for sparsely sampled areas. We now derive the fluid density computation based on the boundary particle volume V_{b_i}.

Even though (3) addresses discontinuities for uniformly sampled particles, it does not account for a variable sampling of particles. Therefore, since the homogeneity of rigid sampling is not guaranteed, (3) causes fluid particles to get large contributions from overly sampled regions. Those overestimated densities cause large pressure forces and therefore stability issues. This is due to the fact that the contribution of boundary particles in (3) does not consider the volume of a particle. This contradicts with the SPH concept, where the contribution of a particle in the approximation of any field variable should be governed by its volume (see (1)). Therefore, we write the contribution of a boundary particle to a fluid particle by taking the volume of the boundary particle into account as

$$\Psi_{b_i}(\rho_0) = \rho_0 V_{b_i}, \tag{5}$$

where ρ_0 denotes the rest density of the fluid that the rigid is interacting with. Finally, the corrected density of a fluid particle can be written in the form

$$\rho_{f_i} = m_{f_i} \sum_j W_{ij} + \sum_k \Psi_{b_k}(\rho_{0_i}) W_{ik}, \tag{6}$$

which computes the densities correctly regardless of the boundary particle sampling. Note that Ψ_b increases the contributions of boundary particles by the amount of the volume ratio of boundary and fluid particles in a uniformly sampled case (by a factor of ~ 1.4). Since Gaussian like kernels are commonly used for SPH simulations, the weight of the next layer of particles is significantly lower compared to the closer layer. Therefore, using a single layer of boundary particles with (6) and taking the missing particles into account in (5) is a decent approximation in practice. See Figure 4 for an illustration of the particle contributions. Our approach updates the contributions of boundary particles for changing boundary configurations with a minimal influence on the fluid particles that are in contact with the boundary. We experimentally verified that even dynamically moving and overlapping boundaries can be handled, which is illustrated in the video corresponding to Figure 5, left.

Even though boundary particles are precomputed, a boundary particle is included in the simulation only if it is in the neighborhood of a fluid particle, similar to [Ihmsen et al. 2010]. For moving boundary particles and all neighboring boundary particles, the represented

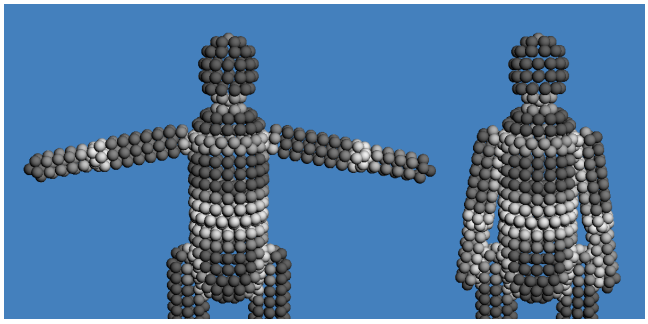

Figure 4: *Color-coded contributions of boundary particles for two ragdolls with different poses. Black and white particles represent large and small contributions, respectively. The contribution is defined by the particular sampling density. Please note, e.g., the smaller contribution of rigid parts in contact.*

particle volumes are recomputed for handling the case of overlapping object parts or objects in close proximity (e.g. for dynamic or kinematic rigid bodies).

2.3 Boundary-Fluid Pressure Force

In SPH, the pressure force between two particles can be directly derived as

$$\mathbf{F}^p_{i\leftarrow j} = -m_i m_j \left(\frac{p_j}{\rho_i \rho_j}\right) \nabla W_{ij}, \tag{7}$$

where p denotes pressure of a particle [Monaghan 2005]. For purely incompressible flow one can say that,

$$\lim_{\eta\to 0}(\rho_i - \rho_j) = 0 \quad \text{and} \quad \lim_{\eta\to 0}(p_i - p_j) = 0$$

where η denotes the density fluctuation of the fluid. Therefore, for weakly compressible fluids, we can assume that $\rho_i \approx \rho_j$ and $p_i \approx p_j$. Consequently, (7) can be approximated as

$$\mathbf{F}^p_{i\leftarrow j} = -m_i m_j \left(\frac{p_x}{\rho_x^2}\right) \nabla W_{ij}, \tag{8}$$

where x can be either i or j. A similar assumption has been also used in the derivation of PCISPH [Solenthaler and Pajarola 2009].

In practice, the applied pressure from fluid to some region of the rigid does not have any kinematic influence on the nearby fluid particles. Based on this fact, we write the pressure force applied from a boundary particle b_j to a fluid particle f_i as

$$\mathbf{F}^p_{f_i\leftarrow b_j} = -m_{f_i} \Psi_{b_j}(\rho_{0_i}) \left(\frac{p_{f_i}}{\rho_{f_i}^2}\right) \nabla W_{ij}, \tag{9}$$

by substituting m_j with $\Psi_{b_j}(\rho_{0_i})$ as done in (6), and using the fluid particle's density and pressure only. The symmetric pressure force from a fluid particle to a boundary particle is

$$\mathbf{F}^p_{b_j\leftarrow f_i} = -\mathbf{F}^p_{f_i\leftarrow b_j}. \tag{10}$$

In (9) and (10), the idea is making use of a fluid particle's own pressure when computing the boundary force. Magnitudes of the boundary forces are based on the pressure of the fluid particle, which increases as the particle gets closer to a boundary. Since the pressure of a fluid particle near a boundary would result in a pressure force to the boundary, that force can be counteracted by a force that is proportional to the pressure of the fluid particle. Therefore,

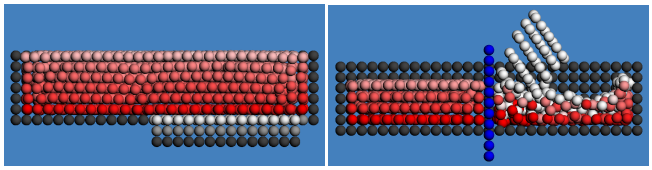

Figure 5: *Handling of overlapping boundaries (left). The negligible interaction of fluid particles on opposite sides of a thin shell (right). Pressures on particles are proportional to their red saturation, black particles denote boundary particles, front side of the box is clipped to make the fluid visible.*

this formulation eliminates sticking artifacts and prevents penetration of fluid particles to the boundaries without using extra forces or position correction. It also eliminates the need for normal information for our boundary particles. Additionally, densities and pressures for boundary particles are not required.

2.4 Boundary-Fluid Friction Force

Inspired by the viscosity-based friction model proposed in [Müller et al. 2004], friction between interacting fluid and boundary particles is generated by employing the laminar artificial viscosity model used in [Monaghan 2005; Becker and Teschner 2007]. It is written as

$$\Pi_{ij} = -\nu \left(\frac{\min(\mathbf{v}_{ij}\cdot\mathbf{x}_{ij},\, 0)}{|\mathbf{x}_{ij}|^2 + \epsilon h^2}\right), \tag{11}$$

with the viscous factor $\nu = \frac{2\alpha h c_s}{\rho_i + \rho_j}$, where α is the viscosity constant, c_s denotes the speed of the numerical propagation, $\mathbf{v}_{ij} = \mathbf{v}_i - \mathbf{v}_j$, $\mathbf{x}_{ij} = \mathbf{x}_i - \mathbf{x}_j$, and $\epsilon = 0.01$ is used to avoid singularities for $|\mathbf{x}_{ij}| = 0$. Finally, the viscosity force between two particles can be computed as

$$\mathbf{F}^v_{i\leftarrow j} = -m_i m_j \Pi_{ij} \nabla W_{ij}. \tag{12}$$

Based on (12), we define the viscosity force from a boundary particle to a fluid particle as

$$\mathbf{F}^v_{f_i\leftarrow b_j} = -m_{f_i} \Psi_{b_j}(\rho_{0_i}) \Pi_{ij} \nabla W_{ij}, \tag{13}$$

with the reformulated viscous factor

$$\nu = \frac{\sigma h c_s}{2\rho_{f_i}}, \tag{14}$$

where σ is the viscosity coefficient between fluid and rigid. From (14), ρ_{b_i} is eliminated based on the same assumption that was used when deriving (9). When computing the viscosity force, the velocity of a boundary particle can be easily computed based on the kinematic properties of the rigid body it belongs to.

The symmetric friction force from a fluid particle to a boundary particle can be written as

$$\mathbf{F}^v_{b_j\leftarrow f_i} = -\mathbf{F}^v_{f_i\leftarrow b_j}. \tag{15}$$

(15) results in drag effects on the rigid (see Figure 6). This idea was also presented in [Becker et al. 2009b]. However, in their work, friction forces are not momentum-conserving.

2.5 Total Force and Force Symmetry

Our boundary particles are transformed based on the position and orientation returned by the rigid solver before computing all relevant forces. Based on the derived forces, the total boundary force

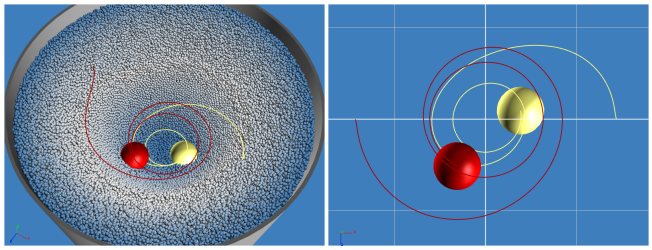

Figure 6: *Two spheres with different fluid viscosities ($\sigma = 0$ for yellow and $\sigma = 8$ for red) are dragged differently by the vortex. Fluid particles are colored according to speed where blue denotes slow particles. The curves visualize the trajectories of the spheres.*

acting on a fluid particle and the total force acting on a boundary particle from its fluid neighbors can be written as

$$\mathbf{F}_{f_i}^{total} = \sum_j \left(\mathbf{F}_{f_i \leftarrow b_j}^{p} + \mathbf{F}_{f_i \leftarrow b_j}^{v} \right),$$
$$\mathbf{F}_{b_i}^{total} = \sum_j \left(\mathbf{F}_{b_i \leftarrow f_j}^{p} + \mathbf{F}_{b_i \leftarrow f_j}^{v} \right).$$

Since the pairwise forces between particles are symmetric (i.e. $\mathbf{F}_{f_i \leftarrow b_j}^{p} + \mathbf{F}_{b_i \leftarrow f_j}^{p} = 0$ and $\mathbf{F}_{f_i \leftarrow b_j}^{v} + \mathbf{F}_{b_i \leftarrow f_j}^{v} = 0$), the total boundary and viscosity forces are symmetric as well, i.e. $\sum_i \mathbf{F}_{f_i}^{total} = \sum_i \mathbf{F}_{b_i}^{total}$.

Afterwards, for each boundary particle i which belongs to a dynamic rigid and has a fluid neighborhood, $\mathbf{F}_{b_i}^{total}$ is converted to total force and torque for the rigid body as

$$\mathbf{F}_{rigid} = \sum_i \mathbf{F}_{b_i}^{total},$$
$$\tau_{rigid} = \sum_i (\mathbf{x}_i - \mathbf{x}^{cm}) \times \mathbf{F}_{b_i}^{total},$$

where $\mathbf{x}^{cm}$ is the center of mass of the rigid body, and $\mathbf{x}_i$ is the position of a boundary particle. Finally, $\mathbf{F}_{rigid}$ and τ_{rigid} are applied to the rigid body.

3 Implementation Details

For the SPH interpolations, we employ the cubic spline kernel [Monaghan 2005]. We use the Euler-Cromer scheme for time integration. We further employ the adaptive time-stepping schemes explained in [Monaghan and Kos 1999] for WCSPH, and [Ihmsen et al. 2010] for PCISPH, where the shock handling criteria in the latter is also added to the former. We also included the velocities of boundary particles inside the time step estimation criteria so as to prevent fluid particles from passing through (i.e. tunnelling). Even though we presented all underlying equations based on Monaghan's pressure and viscosity terms [Monaghan 2005], the same assumptions that we used in our derivations can be applied to different formulations as well, e.g. the force terms in [Müller et al. 2003].

We used Bullet [Coumans 2011] for simulating rigid bodies. However, because of the clear fluid-rigid solver decoupling, any rigid solver might be used as well. For finding neighboring particles, we employed compact hashing as proposed in [Ihmsen et al. 2011]. The application of our two-way coupling approach to SPH is presented in Algorithm 1.

Algorithm 1 Simulation update with our boundary handling model

while *animating* **do**
  foreach *moving-rigid-body i* **do**
    synchronize boundary particles with rigid body state
  foreach *fluid-particle i* **do**
    find fluid and boundary neighbors
    activate neighboring boundary particles
  foreach *fluid-particle i* **do**
    compute density $\rho_i(t)$
    compute pressure $p_i(t)$ (e.g. WCSPH, PCISPH)
  foreach *fluid-particle i* **do**
    add fluid forces $\mathbf{F}_i^{p,\nu,c,ext}(t)$
    add forces exerted by boundary particles $\mathbf{F}_{f_i}^{total}$
  foreach *active-boundary-particle i* **do**
    add forces exerted by fluid particles $\mathbf{F}_{b_i}^{total}$
  foreach *rigid-body i* **do**
    compute the total force exerted by fluids $\mathbf{F}_{rigid_i}$
    compute the total torque exerted by fluids τ_{rigid_i}
  foreach *fluid-particle i* **do**
    update $\mathbf{x}_i, \mathbf{v}_i$
  update rigid bodies (e.g. Bullet)
end while

4 Results

In this section, we demonstrate the versatility of our approach in various simulation settings. If not stated otherwise, we used PCISPH [Solenthaler and Pajarola 2009] as the basic fluid simulation model, where the maximum permissible degree of compression was kept at 1%. In our simulations, we used different particle radii r for different scenarios. The SPH smoothing length was always chosen as $4r$. All simulated fluids had low laminar viscosity ($\alpha = 0.01$) and surface tension ($\kappa = 0.05$), which were determined experimentally to approach the behavior of water. The employed adaptive time-stepping schemes produced time steps roughly between 10^{-2} and 10^{-4}. For all scenes, the computation overhead of the rigid-fluid coupling was mainly between 5-10%. The overhead varied based on the number of fluid-boundary particle pairs. The overhead of the rigid body simulation was usually below 1%. Fluid surfaces were generated using a parallelized implementation [Akinci et al. 2012] of the method proposed in [Solenthaler et al. 2007]. Renderings were done using mental ray v3.9.4 [NVIDIA ARC 2011]. The simulations and renderings were run on an Intel Xeon X5690 with 12 GB RAM. Average computation time per frame (note that for one frame several simulation steps are computed) was 1 second to 1.5 minutes depending on the complexity of the presented scene. These timings exclude surface reconstruction and rendering.

We firstly compare our approach to [Becker et al. 2009b] in a simple setting where a cube with density $400 \frac{kg}{m^3}$ was dropped into a container with 200K fluid particles that have a rest density of $1000 \frac{kg}{m^3}$. We used WCSPH in this example. In contrast to [Becker et al. 2009b], our pairwise forces are symmetric. One frame could be computed in 6 seconds on average with our model, compared to 36 seconds with [Becker et al. 2009b]. The reasons are twofold; our boundary handling allows to use larger time steps (in this experiment three times larger on average), and it does not require additional neighbor queries. This experiment is included in the video corresponding to Figure 7, top-left.

Our viscosity model can simulate drag effects. This is shown in Figure 6 where two spheres with different fluid viscosities were dropped into a whirlpool. The sphere with zero viscosity moved faster to the center of the vortex, while the sphere with high vis-

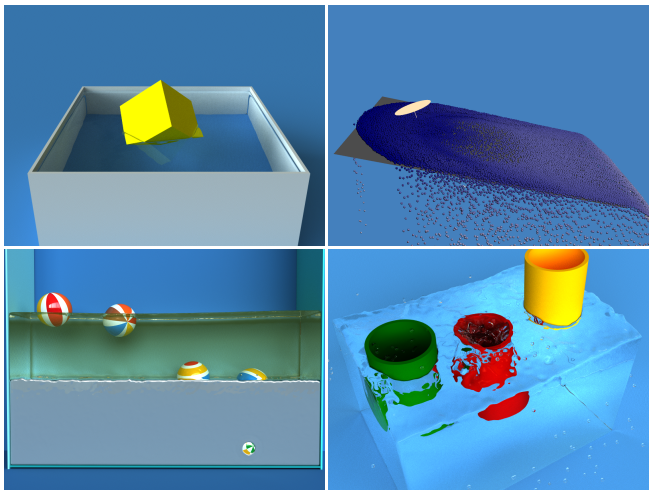

Figure 7: *The simulation setting used for the comparison to [Becker et al. 2009b], where a cube is dropped into water (top-left). The setting for testing different slip conditions (top-right). Six balls with different densities were included in a multi-fluid simulation (bottom-left). Thin shells of different densities, each of them represented by a single particle layer (bottom-right) .*

cosity was dragged by the velocity field of the fluid. In the video corresponding to Figure 7, top-right, we further show in a simple setting that the symmetric force can be used to generate friction on the fluid particles.

One main advantage of our method is that the interaction with lower dimensional rigid bodies can be simulated. Figure 8 shows an example where rods and planes, sampled by a single layer of boundary particles, were dropped into a fluid with 300K particles. Further, we dropped ragdolls that are modeled by multiple capsules connected with different constraints. Even in such challenging scenarios, our two-way coupling approach produces plausible results. Related to the previous example, Figure 7, bottom-right, shows that our approach is able to interact with shell-like structures without interpenetration. In this scene, three cylindrical shells with different densities (which were represented with one layer of boundary particles) interacted with 200K fluid particles.

In order to show that our approach works with multiphase fluids, we simulated two fluids with a density ratio of 1:3 and several spheres with different densities (see Figure 7, bottom-left).

Our approach can handle large density ratios between fluid and rigid bodies. A scene is illustrated in Figure 9, where a sphere with variable density interacted with 90K fluid particles. The density of the sphere was changed from $1\frac{kg}{m^3}$ to $10\frac{kg}{m^3}$, $100\frac{kg}{m^3}$ and $500\frac{kg}{m^3}$. Note that at this point of the sequence, exactly half of the sphere was below the water surface. Finally, the sphere density was changed to $50000\frac{kg}{m^3}$.

A more complex ragdoll example is shown in Figure 10 where 2M fluid particles were used. Due to the dynamics of the individual rigid parts of the ragdoll, the boundary particle sampling can dynamically change in the neighborhood of a fluid particle. The sampling density is, however, considered in our equations so that discontinuities and large forces are prevented. Furthermore, we show a non-uniformly sampled frigate traveling on wavy sea that was simulated using 4M particles (see Figure 3).

In another high resolution example, two towers were modeled using cubes and cylinders. Each cylinder and cube had a density of

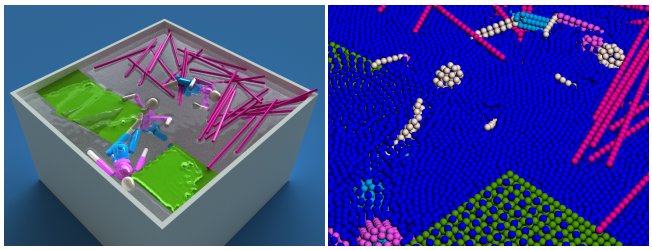

Figure 8: *Handling of lower dimensional objects. The right image shows the underlying particles. Note that planes and rods are modeled with single particle layers.*

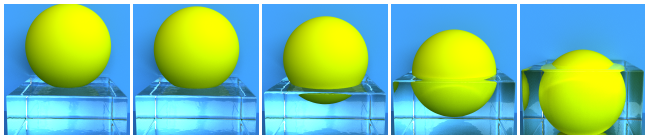

Figure 9: *From left to right, the density of a sphere was slowly increased from* $1\frac{kg}{m^3}$ *to* $50000\frac{kg}{m^3}$.

$600\frac{kg}{m^3}$ and $1500\frac{kg}{m^3}$, respectively. Due to their different densities, primitives interacted differently with the flow that was simulated with up to 2.5M particles (see Figure 11). Finally we show a complex scenario with various rigid objects (see Figure 1). In this scene, two boats filled with ragdolls were dropped into a river like flow. While the second boat was floating, we collapsed the bridge by removing the constraints on both sides of the bridge. Up to 6M fluid particles were used in this simulation.

5 Discussion and Future Work

In our simulations, we generated boundary particles for all rigid bodies including static planar objects (e.g. water containers). For such regions, it would be more efficient to use a wall weight function to approximate the density and force contributions, as done in [Harada et al. 2007]. For complex boundaries with varying triangle size or in non-manifold regions, however, defining a wall weight function is difficult. In those cases, the triangle mesh should be remeshed to get a nearly isotropic triangle distribution. Our boundary particles can be related to such an isotropic triangle mesh, without topology and normal information.

Our approach computes boundary forces based on the pressure of

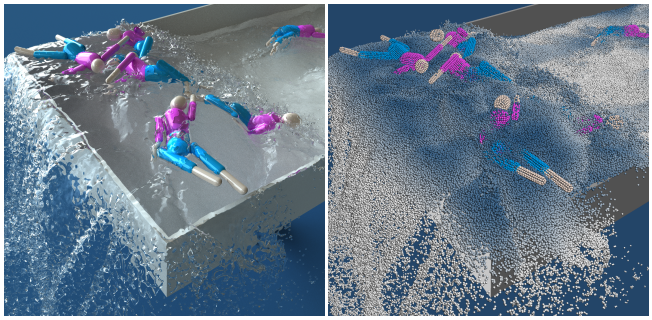

Figure 10: *Dynamically moving rigid bodies in close proximity can change the sampling density in neighborhood of a fluid particle. Since our method takes variable boundary sampling into account, discontinuous forces are prevented.*

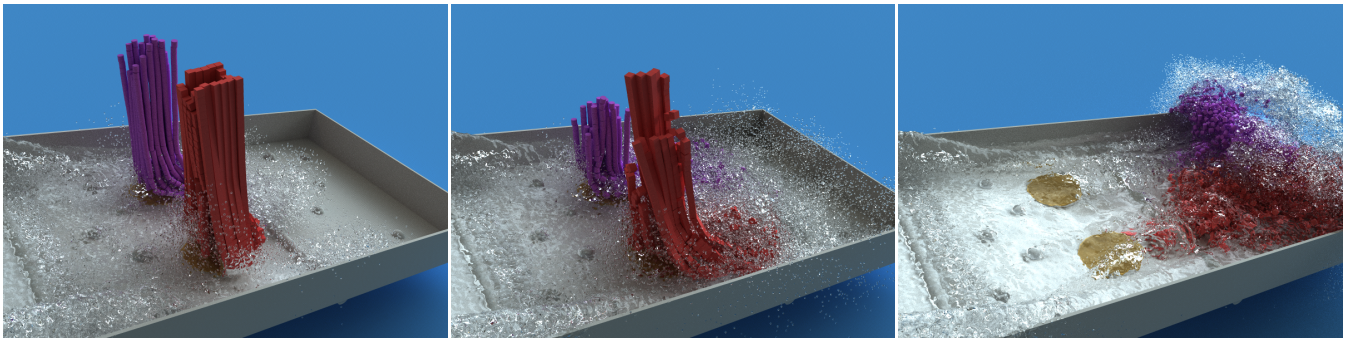

Figure 11: *The approaching water collapses two towers that were modeled by individual cylinders and cubes of different densities.*

fluid particles. While the boundary forces are appropriate for incompressible and weakly compressible fluids, the forces might not be sufficient to prevent interpenetrations when used with compressible fluids. This is particularly the case, if the computed pressure based on a certain density is much smaller for a compressible fluid compared to an incompressible fluid. Further, our approach is limited in terms of a minimal object size that can be handled. The diameter of rods and the thickness of shells cannot be smaller than the diameter of a fluid particle. Thus, the minimum possible object size is defined by the fluid particle resolution. Another issue of our approach is the interaction of fluid particles on opposite sides of thin boundaries. Due to the coupling of minimal thickness of boundaries and particle resolution, these interactions hardly influence the behavior of the fluid as demonstrated in the video corresponding to Figure 5, right. For improperly large time steps (that are larger than what is estimated by the employed adaptive time-stepping schemes), fluid particle tunneling may occur. However, this is a general problem that also exists for fluid-fluid interaction.

We generated the boundary particles such that they are completely enclosed by the rigid. Generating boundary particles exactly at the surface would cause stability issues when fluid particles stuck between two layers of overlapping boundary particles. These issues could be prevented by detecting such fluid particles and treating them differently. In our approach, fluid particles are not immediately updated after the collisions in the final rigid update of Algorithm 1. However, in the next iteration, based on the updated position of the rigid, forces are generated, and the fluid particles are updated. Although our approach outperforms the global approach in [Becker et al. 2009b], we believe that the investigation of alternative global approaches for a simultaneous coupling similar to [Chentanez et al. 2006] is a very promising direction for future research in particle-based fluids.

Our method could also be integrated into previously presented SPH frameworks. One way to employ our approach in [Solenthaler and Gross 2011] would be using two boundary samplings, one for the low resolution simulation and another for the high resolution simulation. Our approach could further be extended to model the two-way coupling of SPH and deformable objects. In case of large deformations, however, potential sampling gaps have to be addressed. Existing unified SPH models such as [Solenthaler et al. 2007; Lenaerts and Dutré 2008] could be used in combination with our model to simulate the interaction of fluid, rigid and deformable models, including thin shells such as cloth.

6 Conclusion

We presented a novel boundary handling method for incompressible SPH fluids that is applicable to both one-way and two-way fluid-rigid coupling. While particle-based solvers offer the benefit that complex boundaries can be handled in a simple way, there is no general agreement how solid-fluid interaction should be handled. Compared to existing techniques like frozen or ghost particles, direct mesh interaction, or penalty forces, our method offers several benefits: Sampling the solids with our proposed boundary particles allows including thin and non-manifold geometries into simulations, since normal information is not needed. Our method does not require a uniform boundary sampling, which facilitates the particle initialization, especially when dealing with complex geometries. Our solution does not only account for the inhomogeneous sampling, but also considers density (and consequently pressure) discontinuities at the boundary as well as symmetry of the forces. Overall, our method adheres to the concept of SPH, is efficient to compute, and allows versatile fluid-rigid coupling.

7 Acknowledgments

This project is supported by the German Research Foundation (DFG) under contract numbers SFB TR8 and TE 632/1. We would like to thank NVIDIA ARC GmbH for their support, Jens Cornelis for his various helps during the project and the reviewers for valuable suggestions that helped to improve the manuscript. The frigate model is courtesy of www.thefree3dmodels.com.

References

ADAMS, B., PAULY, M., KEISER, R., AND GUIBAS, L. 2007. Adaptively sampled particle fluids. *ACM Trans. Graph. (SIGGRAPH Proc.) 26*, 3, 48–54.

AKINCI, G., IHMSEN, M., AKINCI, N., AND TESCHNER, M. 2012. Parallel surface reconstruction for particle-based fluids. *Computer Graphics Forum*, to appear.

ALLARD, J., COURTECUISSE, H., AND FAURE, F. 2011. Implicit FEM and fluid coupling on GPU for interactive multiphysics simulation. In *SIGGRAPH Talks*.

BATTY, C., BERTAILS, F., AND BRIDSON, R. 2007. A fast variational framework for accurate solid-fluid coupling. *ACM Trans. Graph. (SIGGRAPH Proc.) 26*, 3, 100–106.

BECKER, M., AND TESCHNER, M. 2007. Weakly compressible SPH for free surface flows. In *Proc. of the 2007 ACM SIGGRAPH/Eurographics Symposium on Computer Animation*, 209–217.

BECKER, M., IHMSEN, M., AND TESCHNER, M. 2009. Corotated SPH for deformable solids. *Eurographics Workshop on Natural Phenomena*, 27–34.

BECKER, M., TESSENDORF, H., AND TESCHNER, M. 2009. Direct forcing for Lagrangian rigid-fluid coupling. *IEEE Transactions on Visualization and Computer Graphics 15*, 3, 493–503.

BELL, N., YU, Y., AND MUCHA, P. J. 2005. Particle-based simulation of granular materials. In *Proc. of the 2005 ACM SIGGRAPH/Eurographics Symposium on Computer Animation*, 77–86.

BODIN, K., LACOURSIERE, C., AND SERVIN, M. 2011. Constraint fluid. *IEEE Transactions on Visualization and Computer Graphics*, 99, 1–12.

BOTSCH, M., AND KOBBELT, L. 2004. A remeshing approach to multiresolution modeling. In *Proc. of the 2004 ACM SIGGRAPH/Eurographics Symposium on Geometry processing*, 185–192.

CARLSON, M., MUCHA, P., AND TURK, G. 2004. Rigid fluid: animating the interplay between rigid bodies and fluid. *ACM Trans. Graph. (SIGGRAPH Proc.) 23*, 3, 377–384.

CHENTANEZ, N., AND MÜLLER, M. 2010. Real-time simulation of large bodies of water with small scale details. In *Proc. of the 2010 ACM SIGGRAPH/Eurographics Symposium on Computer Animation*, 197–206.

CHENTANEZ, N., GOKTEKIN, T., FELDMAN, B., AND O'BRIEN, J. 2006. Simultaneous coupling of fluids and deformable bodies. In *Proc. of the 2006 ACM SIGGRAPH/Eurographics Symposium on Computer Animation*, 83–89.

CLAVET, S., BEAUDOIN, P., AND POULIN, P. 2005. Particle-based viscoelastic fluid simulation. In *SCA '05: Proceedings of the 2005 ACM SIGGRAPH/Eurographics symposium on Computer animation*, ACM Press, New York, NY, USA, 219–228.

COUMANS, E., 2011. Bullet physics library (version 2.78) [software]. http://www.bulletphysics.org.

DALRYMPLE, R., AND KNIO, O. 2001. SPH modeling of water waves. In *Proc. Coastal Dynamics*, 779–787.

GUENDELMAN, E., SELLE, A., LOSASSO, F., AND FEDKIW, R. 2005. Coupling water and smoke to thin deformable and rigid shells. *ACM Trans. Graph. (SIGGRAPH Proc.) 24*, 3, 973–981.

HARADA, T., KOSHIZUKA, S., AND KAWAGUCHI, Y. 2007. Smoothed particle hydrodynamics on GPUs. In *Proc. of Computer Graphics International*, 63–70.

HU, X., AND ADAMS, N. 2006. A multi-phase SPH method for macroscopic and mesoscopic flows. *Journal of Computational Physics 213*, 2, 844–861.

IHMSEN, M., AKINCI, N., GISSLER, M., AND TESCHNER, M. 2010. Boundary handling and adaptive time-stepping for PCISPH. In *Proc. of VRIPHYS*, 79–88.

IHMSEN, M., AKINCI, N., BECKER, M., AND TESCHNER, M. 2011. A parallel SPH implementation on multi-core CPUs. *Computer Graphics Forum 30*, 1, 99–112.

KEISER, R., ADAMS, B., DUTRÉ, P., GUIBAS, L., AND PAULY, M. 2006. Multiresolution particle-based fluids. Tech. rep., ETH Zurich.

LENAERTS, T., AND DUTRÉ, P. 2008. Unified SPH model for fluid-shell simulations. In *ACM SIGGRAPH 2008 posters*, SIGGRAPH '08, 12:1–12:1.

LENAERTS, T., ADAMS, B., AND DUTRÉ, P. 2008. Porous flow in particle-based fluid simulations. In *SIGGRAPH '08: ACM SIGGRAPH 2008 papers*, ACM, New York, NY, USA, 1–8.

LIBERSKY, L., AND PETSCHEK, A. 1991. Smooth particle hydrodynamics with strength of materials. *Advances in the Free-Lagrange Method Including Contributions on Adaptive Gridding and the Smooth Particle Hydrodynamics Method 395*, 248–257.

MONAGHAN, J., AND KAJTAR, J. 2009. SPH particle boundary forces for arbitrary boundaries. *Computer Physics Communications 180*, 10, 1811–1820.

MONAGHAN, J., AND KOS, A. 1999. Solitary waves on a Cretan beach. *Journal of Waterway, Port, Coastal, and Ocean Engineering 125*, 145.

MONAGHAN, J. 2005. Smoothed particle hydrodynamics. *Reports on Progress in Physics 68*, 8, 1703–1759.

MÜLLER, M., CHARYPAR, D., AND GROSS, M. 2003. Particle-based fluid simulation for interactive applications. In *Proc. of the 2003 ACM SIGGRAPH/Eurographics Symposium on Computer Animation*, 154–159.

MÜLLER, M., SCHIRM, S., TESCHNER, M., HEIDELBERGER, B., AND GROSS, M. 2004. Interaction of fluids with deformable solids. *Computer Animation and Virtual Worlds 15*, 34, 159–171.

NVIDIA ARC, 2011. mental ray 3.9 [software]. http://www.mentalimages.com/products/mental-ray/about-mental-ray.html.

OGER, G., DORING, M., ALESSANDRINI, B., AND FERRANT, P. 2006. Two-dimensional SPH simulations of wedge water entries. *Journal of Computational Physics 213*, 2, 803–822.

OH, S., KIM, Y., AND ROH, B. 2009. Impulse-based rigid body interaction in SPH. *Computer Animation and Virtual Worlds 20*, 2-3, 215–224.

PANIZZO, A. 2004. *Physical and numerical modelling of subaerial landslide generated waves*. PhD thesis, Universita degli studi di L'Aquila, L'Aquila.

RAVEENDRAN, K., WOJTAN, C., AND TURK, G. 2011. Hybrid smoothed particle hydrodynamics. In *Proc. of the 2011 ACM SIGGRAPH/Eurographics Symposium on Computer Animation*, 33–42.

ROBINSON-MOSHER, A., SHINAR, T., GRETARSSON, J., SU, J., AND FEDKIW, R. 2008. Two-way coupling of fluids to rigid and deformable solids and shells. *ACM Trans. Graph. (SIGGRAPH Proc.) 27*, 46:1–46:9.

SOLENTHALER, B., AND GROSS, M. 2011. Two-scale particle simulation. *ACM Trans. on Graphics (SIGGRAPH Proc.) 30*, 4, 81:1–81:8.

SOLENTHALER, B., AND PAJAROLA, R. 2008. Density Contrast SPH Interfaces. In *Proc. of the 2008 ACM SIGGRAPH/Eurographics Symposium on Computer Animation*, 211–218.

SOLENTHALER, B., AND PAJAROLA, R. 2009. Predictive-corrective incompressible SPH. *ACM Trans. on Graphics (SIGGRAPH Proc.) 28*, 3, 1–6.

SOLENTHALER, B., SCHLÄFLI, J., AND PAJAROLA, R. 2007. A unified particle model for fluid-solid interactions. *Computer Animation and Virtual Worlds 18*, 1, 69–82.